

Challenges in piezoelectric force microscopy characterization of sliding ferroelectric WTe_2

Yichen Sun(孙一辰), Luqi Wei(魏鹿奇), Wencheng Fan(范文成), Weihao Sun(孙伟豪), Haonan Wang(王号南), Yaqiong Wang(王亚琼), Zhao Guan(关赵), Wenyi Tong(童文旖), Ke Qu(屈可), Zhenzhong Yang(杨振中), Binbin Chen(陈斌斌), Pinghua Xiang(向平华), Chungang Duan(段纯刚), and Ni Zhong(钟妮)

Citation: Chin. Phys. B, 2026, 35 (**7**): 077701. DOI: 10.1088/1674-1056/ae56e6
http://cpb.iphy.ac.cn; http://iopscience.iop.org/cpb

What follows is a list of articles you may be interested in

Design of electrocaloric materials based on *E-T* phase diagrams

Fei Han(韩飞), Rongju Zhong(钟容菊), Jikun Yang(杨继昆), Chuanbao Liu(刘传宝), and Yang Bai(白洋)
Chin. Phys. B, 2026, 35 (**2**): 027704. DOI: 10.1088/1674-1056/ae3308

Improved ferroelectricity in Mn-doped HfO_2 (111) epitaxial thin films through controlled doping and substrate orientation

Jiayi Gu(顾嘉仪), Haiyi Zhang(张海义), Weijin Pan(潘炜进), Haifeng Bu(卜海峰), Zhijian Shen(沈志健), Shengchun Shen(沈胜春), Yuewei Yin(殷月伟), and Xiaoguang Li(李晓光)
Chin. Phys. B, 2025, 34 (**8**): 087701. DOI: 10.1088/1674-1056/add1bc

Manipulating optical and electronic properties through interfacial ferroelectricity

Yulu Liu(刘钰璐), Gan Liu(刘敢), and Xiaoxiang Xi(奚啸翔)
Chin. Phys. B, 2025, 34 (**1**): 017701. DOI: 10.1088/1674-1056/ad9456

Observing ferroelastic switching in $Hf_{0.5}Zr_{0.5}O_2$ thin film

Zhao Guan(关赵), Tao Wang(王陶), Yunzhe Zheng(郑赟喆), Yue Peng(彭悦), Luqi Wei(魏鹿奇), Yuke Zhang(张宇科), Abliz Mattursun(阿卜力孜 cdot 麦提图尔苏), Jiahao Huang(黄家豪), Wen-Yi Tong(童文旖), Genquan Han(韩根全), Binbin Chen(陈斌斌), Ping-Hua Xiang(向平华), Chun-Gang Duan(段纯刚), and Ni Zhong(钟妮)
Chin. Phys. B, 2024, 33 (**6**): 067701. DOI: 10.1088/1674-1056/ad362f

Sr-doping effects on conductivity, charge transport, and ferroelectricity of $Ba_{0.7}La_{0.3}TiO_3$ epitaxial thin films

Qiang Li(李强), Dao Wang(王岛), Yan Zhang(张岩), Yu-Shan Li(李育珊), Ai-Hua Zhang(张爱华), Rui-Qiang Tao(陶瑞强), Zhen Fan(樊贞), Min Zeng(曾敏), Guo-Fu Zhou(周国富), Xu-Bing Lu(陆旭兵), and Jun-Ming Liu(刘俊明)
Chin. Phys. B, 2021, 30 (**2**): 027701. DOI: 10.1088/1674-1056/abc15a

---

SPECIAL TOPIC — Multiferroicity and multicaloric effects

Challenges in piezoelectric force microscopy characterization of sliding ferroelectric WTe_2

Yichen Sun(孙一辰)[1], Luqi Wei(魏鹿奇)[1], Wencheng Fan(范文成)[1], Weihao Sun(孙伟豪)[1], Haonan Wang(王号南)[1], Yaqiong Wang(王亚琼)[1], Zhao Guan(关赵)[1], Wenyi Tong(童文旖)[1], Ke Qu(屈可)[1], Zhenzhong Yang(杨振中)[1], Binbin Chen(陈斌斌)[1], Pinghua Xiang(向平华)[1,2], Chungang Duan(段纯刚)[1,2], and Ni Zhong(钟妮)[1,2,†]

[1] *Key Laboratory of Polar Materials and Devices (MOE), Shanghai Center of Brain-inspired Intelligent Materials and Devices, Department of Electronics, East China Normal University, Shanghai* 200241, *China*

[2] *Collaborative Innovation Center of Extreme Optics, Shanxi University, Taiyuan* 030006, *China*

(Received 21 February 2026; revised manuscript received 19 March 2026; accepted manuscript online 25 March 2026)

Sliding ferroelectricity, an emerging ferroelectric mechanism in 2D systems whose polarization arises from interlayer charge transfer, has attracted considerable attention due to its unique switching behavior, such as superior endurance and high switching speed. However, its experimental characterization remains challenging due to the low polarizability and technical difficulties. Using piezoelectric force microscopy (PFM), we investigate T_d-WTe_2 as a model sliding ferroelectric system, aiming to fill the gap in the characterization of sliding ferroelectricity from a microscopic perspective. We observed ferroelectric-like PFM phase contrast and amplitude hysteresis in few-layer (1–4 L) WTe_2 flakes under ambient conditions, in contrast to the theoretical predictions for flakes thicker than 2 L. Surface oxidation of WTe_2 has been identified by Raman and other characterization techniques. Therefore, similar PFM characterization has been carried out on the flakes covered by h-BN, which prevented WTe_2 from oxidation, and no ferroelectric behavior could be found. Consequently, the ferroelectric-like PFM phenomena are attributed to oxidation rather than intrinsic ferroelectricity in WTe_2. Combined with analyses of PFM testing principles and the mechanism of sliding ferroelectricity, we identify the limitations and challenges of PFM in characterizing sliding ferroelectricity. This work provides valuable insights for the subsequent characterization and application of related sliding ferroelectrics.

Keywords: 2D ferroelectric, sliding ferroelectric, piezoelectric force microscopy (PFM)

PACS: 77.80.–e, 77.90.+k, 77.80.Dj

DOI: 10.1088/1674-1056/ae56e6 **CSTR:** 32038.14.CPB.ae56e6

Two-dimensional (2D) ferroelectric materials break through the limitations of traditional three-dimensional material rules by possessing atomic-level thickness and layer stacking properties.[1] The polarization switching of conventional ferroelectrics is achieved by displacement of ions in the lattice, whereas the ferroelectricity of sliding ferroelectrics arises when two layers adopt a specific stacking configuration, which breaks the central symmetry.[2–4] At this point, the charge between the layers is redistributed, producing a spontaneous polarization perpendicular to the plane.[5,6] This polarization relies on the relative sliding of two layers as a whole in a specific direction under the action of an external electric field. The interlayer interface between the layered materials and the weak interlayer van der Waals (vdW) forces provide the possibility of interlayer sliding.[7] Thus, sliding ferroelectricity, a completely new ferroelectric mechanism, emerges. This unique polarization switching mechanism gives sliding ferroelectrics a series of excellent properties such as high fatigue resistance,[8] fast and low-power polarization switching,[9,10] and so on. In recent years, there have been continuous reports on the discovery and characterization of sliding ferroelectrics in artificially stacked twisted hexagonal boron nitride (h-BN),[11–14] graphene,[15] homo[16,17] and hetero[18] junctions of transition metal dichalcogenides (TMDCs), which could be classified as moiré ferroelectrics.[19] They exhibit sliding ferroelectricity when stacked in parallel (AB′ stack or BA′ stack), and complex edge polarization topology,[14,20–22] In addition to artificially stacked moiré ferroelectrics, there exist intrinsic sliding ferroelectrics that occur naturally in certain crystal structures, including WTe_2,[23–25] 3R-MoS_2,[17,26,27] 1T′-ReS_2,[28] Cd_3Cl_6,[29] InSe,[30] etc.

WTe_2 with a distorted 1T′ phase (T_d-WTe_2, orthorhombic, space group *Pnm*21) has attracted extensive attention for its remarkable properties, including nonlinear anomalous Hall effect,[31] huge unsaturated magnetoresistance,[32] quantum spin Hall state,[33] topological features,[34] and superconductivity.[35] Interestingly, T_d-WTe_2 was recently reported as a switchable polar metal, a material that combines switchable electric polarization (typically found in insulators) with metallic conductivity, which was measured through the change of conductivity induced by polarization switching under a vertical electric field in a dual-gate de-

†Corresponding author. E-mail: nzhong@ee.ecnu.edu.cn

© 2026 Chinese Physical Society and IOP Publishing Ltd. All rights, including for text and data mining, AI training, and similar technologies, are reserved.

vice configuration.[23] Density functional theory (DFT) calculations have revealed that the ferroelectric polarization of T_d-WTe_2 arises from interlayer charge redistribution.[6] *In situ* gate-dependent second-harmonic generation (SHG) and Raman spectroscopy studies exhibited electrically driven stacking transitions in T_d-WTe_2.[36] Capacitive behavior in a dual-gate mesoscopic device was characterized to directly measure the spontaneous polarization in the bilayer T_d-WTe_2.[37] It should be noted that all these studies have observed the polarization switching of WTe_2 at the macroscopic level, and microscopic evidence of the sliding ferroelectric switching mechanism in WTe_2 remains limited, particularly regarding real-space observation of polarization switching via conventional PFM.[24]

In the current work, we systematically investigate sliding ferroelectricity in T_d-WTe_2 using a PFM technique under atmospheric conditions. Through amplitude and phase hysteresis measurements, as well as tip-induced switching in few-layer WTe_2, we unexpectedly observe ferroelectric-like signals not only in multilayers but also in monolayer T_d-WTe_2, which challenges the bilayer thickness limitation of sliding ferroelectrics. The stability of few-layer T_d-WTe_2 in atmosphere is investigated, and oxidation is verified by Raman spectroscopy. To explore the relationship between the oxidation effect and the ferroelectric-like PFM results, we perform a comparative measurement on the T_d-WTe_2 covered with a thin h-BN layer, and the ferroelectric-like signals disappeared. The complete suppression of ferroelectric-like PFM signals in h-BN-protected T_d-WTe_2 unambiguously links the ferroelectric-like phenomena to surface oxidation effects rather than intrinsic ferroelectricity. Our findings provide critical insights for PFM characterization of sliding ferroelectrics, and highlight the necessity of distinguishing intrinsic polarization from measurement artifacts.

To prepare high-quality few-layer samples, we exploited the strong interfacial energy between transition metal dichalcogenides and metals compared to van der Waals interactions[38–40] by sputtering 2 nm Ti/4 nm Au on a 300 nm SiO_2/Si substrate to exfoliate WTe_2 with PDMS/tape (Fig. 1(b), top). This gold-assisted method results in large-area few-layer flakes with sizes as large as 150×800 μm^2, as shown in Fig. 1(b) (bottom). The Raman spectra of mechanically exfoliated flakes are shown in Fig. 1(c) (top) with seven characteristic peaks: $^2A_1$ (80 cm^{-1}), $^2A_2$ (88 cm^{-1}), $^3A_2$ (109 cm^{-1}), $^3A_1$ (119 cm^{-1}), $^4A_1$ (134 cm^{-1}), $^8A_1$ (163 cm^{-1}), and $^{10}A_1$ (213 cm^{-1}), matching theoretical predictions of T_d-WTe_2 belonging to the space point group *Pmn*21 with a total of 17 Raman-active modes[41] (11 A_1 and 6 A_2). Second harmonic generation measurements (Fig. 1(d)) on PMMA-encapsulated samples further verified the non-centrosymmetric structure at room temperature.[42] An atomic-scale high-angle annular dark field scanning transmission electron microscopy (HAADF-STEM) investigation was further conducted to confirm the atomic structure of T_d-WTe_2. A 4 LT$_d$-WTe_2 exfoliated on gold is shown in Fig. 1 (top), as well as the locally enlarged atomic-scale image corresponding to the schematic diagram of the *c*–*b* cross-sectional structure (Fig. 1(e) bottom).

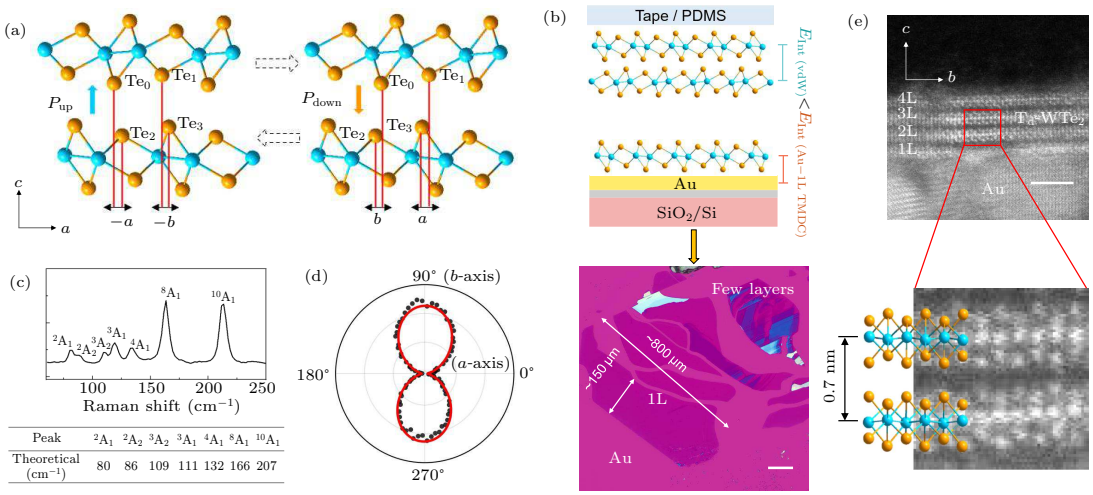


Fig. 1. (a) Schematic diagram of interlayer sliding in bilayer T_d-WTe_2. (b) Schematic diagram of gold-assisted exfoliation (top). Optical image of T_d-WTe_2 exfoliated by gold-assisted method (bottom). Scale bar, 100 μm. (c) Raman spectra of T_d-WTe_2: WTe_2 nanosheets at room temperature with excitation light wavelength of 532 nm (upper part). Theoretical values of seven peaks of T_d-WTe_2 (lower part). (d) Angular polar diagram of SHG signal (parallel) of WTe_2 nanosheets at room temperature, excitation light wavelength is 515 nm. (e) HAADF-STEM image of T_d-WTe_2 exfoliated on gold along *c*–*b* plane (top). Scale bar, 2 nm. The locally enlarged atomic-scale image and atomic-structure schematic diagram of T_d-WTe_2 (bottom).

PFM is widely recognized as a powerful technique for characterizing the ferroelectric properties of materials at the nanoscale volume.[43,44] Its core principle is based on the inverse piezoelectric effect. When an alternating voltage is applied to the surface of a piezoelectric (ferroelectric) material via a conductive probe, the material undergoes corresponding periodic mechanical deformation (expansion or contraction). The displacement signal of the cantilever is amplified

by a lock-in amplifier to obtain amplitude (reflecting the magnitude of deformation) and phase (reflecting changes in polarization direction) information. In the current work, we employed dual AC resonance tracking (DART) PFM to study T_d-WTe_2, utilizing two complementary modes: (1) hysteresis mode, which combines a small AC probe signal with a slow DC bias ramp (0.001–3 Hz) to generate characteristic butterfly amplitude curves and 180° phase hysteresis loops (Fig. 2(a)), and (2) write-read mode involving local poling via a biased tip scanning ($\pm V_{dc}$) followed by mapping of amplitude and phase variations.

T_d-WTe_2 was exfoliated onto conductive substrates via the above-mentioned gold-assisted exfoliation, which provided samples with varying thicknesses for PFM measurements. Atomic force microscopy (AFM) was first employed to confirm the thickness of the flakes (Fig. 2(b)), revealing the expected ~ 0.7 nm step height per van der Waals layer.[6] Subsequently, PFM amplitude and phase hysteresis loops of few-layer samples (2–4 layers) were acquired, as presented in Figs. 2(c) and 2(d). Distinct butterfly-shaped amplitude curves and 180° phase flips were observed in samples with 2–4 layers, consistent with the characteristics of ferroelectricity. Intriguingly, similar ferroelectric-like signals were also detected in a monolayer, raising fundamental questions about whether these ferroelectric-like responses originate from intrinsic ferroelectricity or alternative mechanisms.[45] To further investigate this phenomenon, we performed localized poling using ±3 V biases on 3 nm WTe_2 through the conductive tip during surface scanning, illustrated as a white square in Fig. 2(e). Immediately after poling, a notable reduction in amplitude response was observed in the −3 V poled region (Fig. 2(g)), along with a phase difference of approximately 130° between +3 V and −3 V regions (Fig. 2(f)). Another key characteristic of ferroelectrics is the formation of domain walls. After applying voltages of opposite directions to adjacent regions, distinct domain walls would form at the boundary between these regions in a real ferroelectric. Notably, amplitude minima, which are characteristic of ferroelectric domain walls, were absent between positive and negative poled regions (Fig. 2(g)). Moreover, the modified phase contrast gradually diminished (Fig. 2(h)) and nearly vanished within one hour, indicating a volatile behavior[46] that is fundamentally distinct from the non-volatile polarization switching of conventional ferroelectrics.[45] It suggests that the ferroelectric-like characteristics (Figs. 2(c), 2(d), 2(f), and 2(g)) probably originated from charge injection effects[47,48] rather than intrinsic ferroelectricity, which could be incompatible with the metallic nature of T_d-WTe_2.

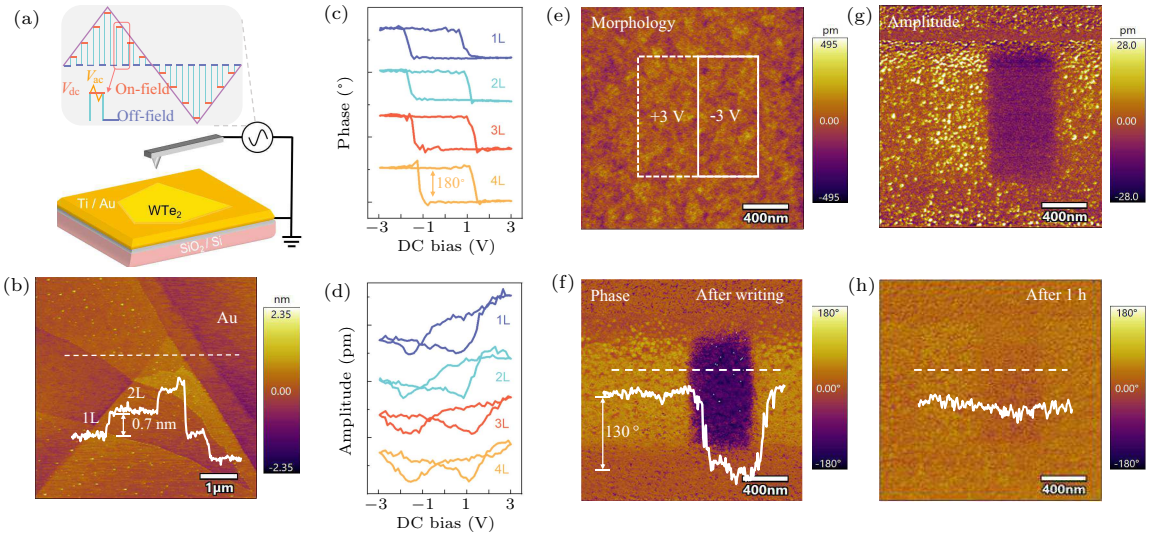


Fig. 2. Out-of-plane piezoelectric responses of T_d-WTe_2 thin flakes. (a) Schematic diagram of PFM measuring experimental apparatus. The inset shows the voltage waveforms used in the measurements. (b) Morphology of T_d-WTe_2 thin layers exfoliated on a gold substrate. The inset shows the height of white dashed line. (c) PFM phase hysteresis and (d) butterfly-shaped PFM amplitude-voltage loops of T_d-WTe_2. (e) Morphology of WTe_2 after bias voltage writing. The white square represents the regions where +3 V and −3 V voltages were applied. (g) PFM amplitude mapping and (f) phase images after writing, and (h) phase image 1 h after writing. The inset shows the phase difference of cross-sectional profiles.

Previous reports have indicated that WTe_2 is sensitive to oxygen exposure,[49] and an oxide layer forms on its surface under ambient conditions. We further analyze the oxidation of few-layer WTe_2 samples exposed to air by Raman spectroscopy, as shown in Fig. 3(a). It is noted that four distinct Raman peaks can be observed in a fresh exfoliated sample, which degrade rapidly upon air exposure and completely disappear after 30 minutes, indicating full oxidation. Quantitative analysis using the $^8A_1$ peak intensity as an oxidation marker shows a significant decay of the monolayer sample (Fig. 3(b)). Complementary Kelvin probe force microscopy (KPFM) (Fig. S1 in supplementary material) and electrostatic force microscopy (EFM) (Fig. S2 in supplementary material) measurements also confirm this thickness-dependent behavior. The rapid transi-

tion of few-layer WTe_2 to an insulating state upon exposure to air suggests that oxidation primarily occurs on the surface, where both W and Te react with oxygen and eventually form amorphous WTe_2O_x.[24] Figure 3(e) shows the STEM image of WTe_2 after exposure to air for a period of time. As shown in the figure, the surface of WTe_2 is oxidized and becomes amorphous, while the underlying WTe_2 still maintains a well-defined crystal lattice structure. Once the surface oxide layer is formed, it acts as a protective shield on the underlying layers to prevent further degradation, as illustrated in Fig. 3(f). Correspondingly, in Fig. 2(b), the height between layers remains 0.7 nm.

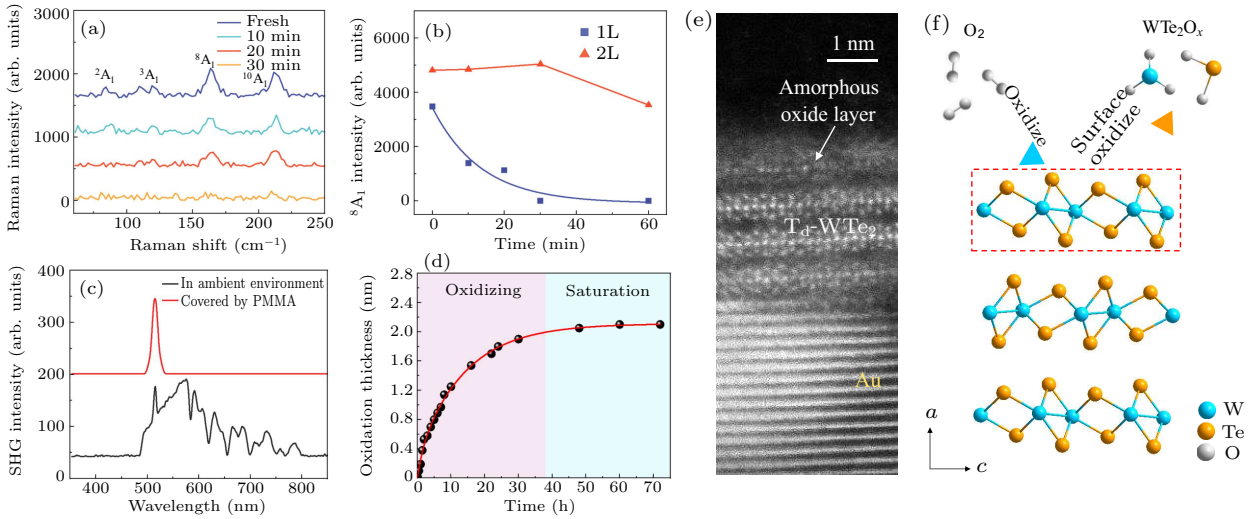


Fig. 3. (a) Degradation of Raman spectra of monolayer WTe_2 in ambient environment. (b) Decay of the $^8A_1$ peak signal intensity over time for mono- and bi- layer WTe_2. (c) SHG signals of WTe_2 exposed to the air (black line) and the one encapsulated by PMMA immediately after exfoliation (red line). (d) Growth of WTe_2 oxide layer thickness in ambient environment over time. (e) STEM images of WTe_2 after exposure to air for a period of time. (f) Schematic diagram of surface oxidation of WTe_2.

As a measurement technique, SHG is highly sensitive to surface symmetry, so amorphous surface oxide layers can have a serious impact on the results. Figure 3(c) compares samples encapsulated with PMMA immediately after exfoliation (red line) and unencapsulated ones (black line). The wavelength of the second harmonic peak is 515 nm. Due to the influence of the surface oxide layer, the signal of the unencapsulated sample exhibits severe noise interference in addition to the conventional second harmonic signal. Defining the oxide layer thickness as the actual thickness $d(t)$ – initial thickness $d(0)$, under the ambient environment in our laboratory, the oxide layer thickness of WTe_2 approaches saturation after approximately 40 minutes, with the final thickness stabilizing around 2 nm (Fig. 3(d)). The surface roughness also increased significantly (Fig. S3 in supplementary material). Therefore, the ferroelectric-like phenomenon observed in previous PFM tests is highly likely attributed to the influence of the surface oxide layer. Numerous factors and measurement artifacts, such as charge injection,[48] electrostatic effects,[47] mechanical variations, and electrochemical responses,[50] may affect the results of PFM characterization. When the voltage-biased tip comes into contact with the oxidized surface, large amounts of charges are injected. Signals resembling ferroelectricity were detected in the amplitude and phase mappings immediately after voltage writing. However, these signals gradually weaken and eventually vanish over time. The most likely cause of this result is charge injection in the oxide layer.[50] Further experiments are required to clarify the origin of the ferroelectric-like signal. Nevertheless, we can conclude that this ferroelectric-like signal does not originate from the intrinsic ferroelectricity of WTe_2. Our findings demonstrate that surface oxidation of few-layer T_d-WTe_2 occurs unavoidably during ambient characterization following exfoliation. The oxidation effect introduces significant artifacts that cannot be neglected in PFM measurements.

To further eliminate the impact of such degradation, few-layer WTe_2 was first exfoliated in a nitrogen-filled glovebox (with H_2O and O_2 levels below 0.5 ppm) and subsequently encapsulated with ultrathin insulating h-BN via dry transfer[51] (details in supplementary material). The encapsulated samples were taken out of the glovebox for PFM measurements, as shown in Fig. 4(a). The reason for choosing an extremely thin thickness is to prevent the dielectric layer of a certain thickness from hindering the detection of signals from WTe_2.[52,53] The thickness of BN is about 1.2 nm, as shown in Fig. S6. To verify that BN encapsulation does not affect the measurement of ferroelectric signals by PFM, we performed PFM measurements on $CuInP_2S_6$ (CIPS) with and without BN coverage, as shown in Fig. S7. The results indicate that BN does not influence the characterization of the underlying ferroelectric domain structure by PFM, and the domains and domain walls of CIPS are observed to be continuous across the BN step edge. Further-

more, we performed polarization switching measurements on BN-covered CIPS, as shown in Fig. S8. The results indicate that even with a 6 nm-thick BN layer, the tip electric field can still write domains into CIPS and realize PFM read and write measurements.

Prior to measurement, contact mode was used to eliminate the bubbles at the BN–WTe_2 interface formed during transfer, ensuring optimal contact and improving surface flatness. This two-dimensional van der Waals contact with quite low interface defect density and fewer dangling bonds helps to achieve higher interface cleanliness, providing a clean interface to minimize experimental artifacts. A comparison of PFM amplitude and phase responses of unencapsulated (red line) and h-BN-encapsulated (black) bilayer WTe_2 is shown in Fig. 4(b). It can be clearly observed that the butterfly-shaped amplitude and phase hysteresis loops were not detected in the h-BN-encapsulated WTe_2. In contrast, the test results of unencapsulated WTe_2 were consistent with those in Figs. 2(c) and 2(d). Figure 4(c) summarizes the phase difference results of PFM tests from mono- to four-layer WTe_2 under both encapsulated and unencapsulated conditions, with error bars representing the variance across multiple measurements. The absence of 180° phase difference in encapsulated few-layer WTe_2 indicates that the ferroelectric-like phenomenon observed in pristine WTe_2 most likely arises from surface oxidation rather than intrinsic ferroelectricity.[45,50] As mentioned in some previous reports, butterfly hysteresis loops and 180° phase differences can also be measured in non-ferroelectric materials using PFM; the presence of these two phenomena is not sufficient evidence for the existence of ferroelectricity.[54,55] To verify the sliding ferroelectricity of T_d-WTe_2, we fabricated a device similar to the one reported in Fei's work.[23] The vertical electric field formed by two gates was used to modulate the polarization of WTe_2, and bistable states characteristic of ferroelectricity were observed in its transport curves, as shown in Fig. S9.

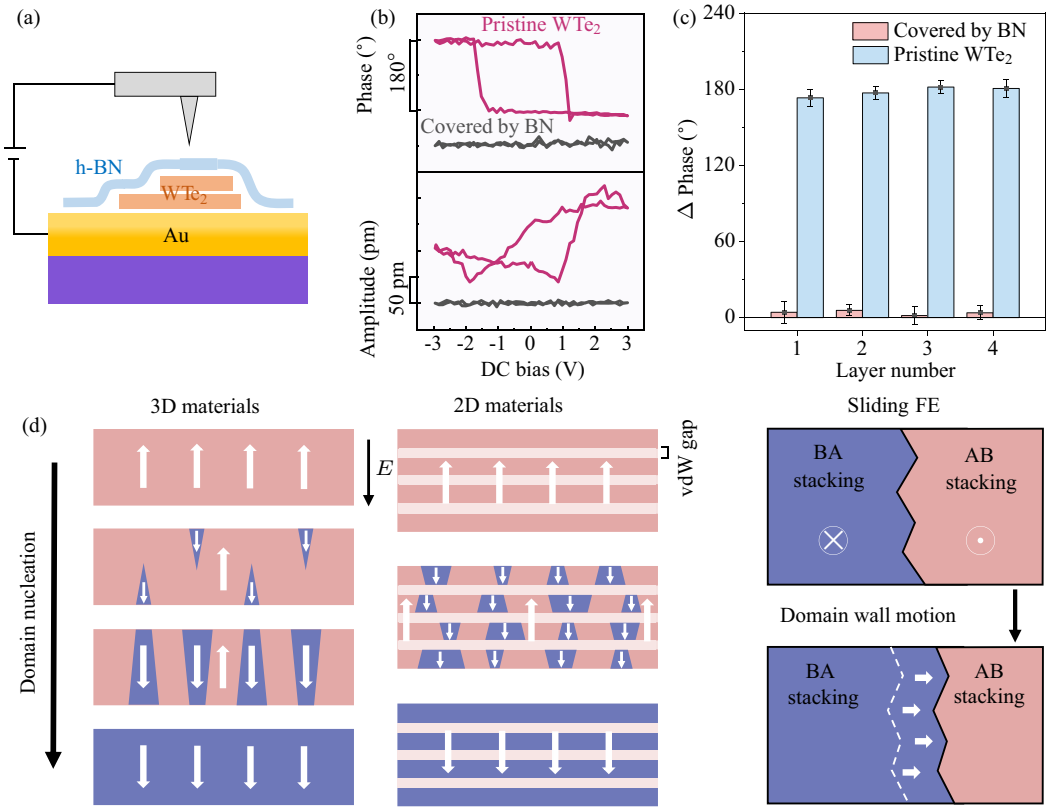


Fig. 4. (a) Schematic diagram of PFM tests on WTe_2 encapsulated by h-BN. (b) PFM phase hysteresis and (c) butterfly-shaped PFM amplitude-voltage loops of bilayer T_d-WTe_2 (red) and the one covered by BN (grey). (c) PFM phase difference of 1–4-layer T_d-WTe_2 without and with BN encapsulation. (d) Schematic diagram of polarization switching mechanisms in traditional 3D ferroelectrics (left), 2D ferroelectrics (center), and sliding ferroelectrics (right).

From another perspective, PFM inherently faces certain challenges and limitations in characterizing the sliding ferroelectricity of WTe_2. As shown in Fig. 4(d), the polarization switching of traditional three-dimensional ferroelectrics (left), such as PZT, undergoes three processes under the action of an external electric field, including nucleation, growth, and complete switching.[56] Similarly, typical two-dimensional van der Waals ferroelectrics like $CuInP_2S_6$ (CIPS) (middle) exhibit similar behaviors: their ferroelectricity mainly stems from the directional displacement of intra-layer ions. However, van der Waals gaps in layered materials disrupt the continuity of domain growth, leading to independent nucleation and growth in each layer;[57] nonetheless, they ultimately achieve overall polarization switching. As a microscopic characterization tech-

nique, PFM can probe the nucleation, growth, and local polarization switching in both traditional three-dimensional ferroelectrics and two-dimensional van der Waals ferroelectrics through local voltage poling by a conductive tip, with domain walls visible in amplitude mappings.[50] However, the mechanism of sliding ferroelectricity (right) significantly differs from the above. Unlike displacement-type ferroelectrics, sliding ferroelectricity originates from interlayer translation rather than ionic displacement, exhibiting distinct switching dynamics. Previous experimental[11,16,19,58,69] and theoretical[60–65] works show that the transition region (domain wall) plays an important role in polarization switching of sliding ferroelectrics. Most reported observations of sliding ferroelectricity occur in artificially stacked or twisted 2D vdW heterostructures, where the switching phenomenon of sliding ferroelectrics is more commonly observed in the form of domain wall motion,[16,59,66–68] while it is difficult to achieve switching through nucleation and growth by applying an external electric field.[11,60–62] Liu's group has summarized recent reports on sliding ferroelectricity. The evidence for sliding ferroelectricity is mainly obtained from two approaches: electric-field-modulated transport characteristics using dual-gate devices, and domain wall motion under stress or an electric field.[2] In the experiments of this work, domain wall information was not observed in all the PFM measurements (Fig. S4 in supplementary material). Additionally, no polarization accumulation phenomenon or different polarization states similar to those in 3R-MoS_2[17] were detected in the results of KPFM (Fig. S5 in supplementary material), which is in accordance with theoretical expectations.[69]

Unlike conventional ferroelectrics, which are usually insulators, T_d-WTe_2 exhibits semimetal behavior. Charge screening resulting from conductivity will interfere with PFM results. Meanwhile, the polarization of WTe_2 is extremely small[6] ($\sim 5.1 \times 10^{-2}$ μC·cm^{-2}). Furthermore, as shown in this article, WTe_2 is fragile and easily oxidized in air. Since unavoidable exposure to air occurs during sample preparation and measurement, it is highly challenging to preserve its stability and obtain its intrinsic properties. These factors further increase the difficulty of PFM experiments, and they well explain our experimental observations where conventional PFM failed to detect unambiguous evidence of ferroelectric switching in WTe_2.

We performed piezoelectric force microscopy measurements on monolayer to four-layer T_d-WTe_2 at room temperature and observed ferroelectric-like phenomena in amplitude, phase, and write–read tests. Subsequent measurements on unoxidized T_d-WTe_2 encapsulated with ultrathin h-BN failed to reproduce the butterfly-shaped amplitude and phase hysteresis loops. Results from Raman spectroscopy and SHG further confirmed that unencapsulated samples are highly susceptible to oxidation in air, suggesting that the ferroelectric-like phenomena may be affected by the surface oxide layer. Finally, by integrating the interlayer sliding and domain movement mechanisms of sliding ferroelectricity, the testing principle of PFM, and the intrinsic properties of WTe_2, we summarized the limitations and challenges in characterizing the sliding ferroelectricity of T_d-WTe_2 via PFM. This also provides us with an important insight: the observation and confirmation of sliding ferroelectricity cannot rely solely on PFM results, but require joint verification through other methods and approaches.

Acknowledgements

This work was supported by the National Key Research and Development Program of China (Grant Nos. 2024YFA14097000 and 2022YFA1402902), the National Natural Science Foundation of China (Grant Nos. 12474084, 12134003, 12374145, and 12574192), Chenguang Program of Shanghai Education Development Foundation and Shanghai Municipal Education Commission, ECNU (East China Normal University) Multifunctional Platform for Innovation (006, 001), and the Fundamental Research Funds for the Central Universities.

References

[1] Guan Z, Hu H, Shen X, Xiang P, Zhong N, Chu J and Duan C 2020 *Adv. Electron. Mater.* **6** 1900818
[2] Yang F, Pan E, Liu Q, Tapasztó L, He Y, Luo X and Liu F 2026 *Sci. China Mater.* **69** 1918
[3] Wu M and Li J 2021 *Proc. Natl. Acad. Sci. USA* **118** e2115703118
[4] Zhi A, Chen Z, Wang J, Xu H, Miao G, Chen P, Han H, Cai C, Li X, Yu G, Wang W, Wang L, Tian X and Bai X 2025 *Chin. Phys. Lett.* **42** 070717
[5] Li L and Wu M 2017 *ACS Nano* **11** 6382
[6] Yang Q, Wu M and Li J 2018 *J. Phys. Chem. Lett.* **9** 7160
[7] Butler S Z, Hollen S M, Cao L, Cui Y, Gupta J A, Gutiérrez H R, Heinz T F, Hong S S, Huang J, Ismach A F, Johnston-Halperin E, Kuno M, Plashnitsa V V, Robinson R D, Ruoff R S, Salahuddin S, Shan J, Shi L, Spencer M G, Terrones M, Windl W and Goldberger J E 2013 *ACS Nano* **7** 2898
[8] Bian R, He R, Pan E, Li Z, Cao G, Meng P, Chen J, Liu Q, Zhong Z, Li W and Liu F 2024 *Science* **385** 57
[9] Bai Y, Yu Z, Guan Z, Tian J, Wang C, Yao X, Yang Y, Lei Y, Xu J, Liu C, Zhu J, Tu Y, Shen S, Xiang H, Li X, Xu C and Wang J 2025 *Nat. Commun.* **16** 7221
[10] Yasuda K, Zalys-Geller E, Wang X, Bennett D, Cheema S S, Watanabe K, Taniguchi T, Kaxiras E, Jarillo-Herrero P and Ashoori R 2024 *Science* **385** 53
[11] Vizner Stern M, Waschitz Y, Cao W, Nevo I, Watanabe K, Taniguchi T, Sela E, Urbakh M, Hod O and Ben Shalom M 2021 *Science* **372** 1462
[12] Yasuda K, Wang X, Watanabe K, Taniguchi T and Jarillo-Herrero P 2021 *Science* **372** 1458
[13] Fan W C, Wei L Q, Tong W Y, Guan Z, Xu H W, Sun W H, Tian M, Wan N, Chen B B, Xiang P H, Duan C G and Zhong N 2026 *Adv. Funct. Mater.* **36** e74888
[14] Fan W C, Guan Z, Wei L Q, Xu H W, Tong W Y, Tian M, Wan N, Yao C S, Zheng J D, Chen B B, Xiang P H, Zhong N and Duan C G 2025 *Nat. Commun.* **16** 3557
[15] Zheng Z, Ma Q, Bi Z, de la Barrera S, Liu M H, Mao N, Zhang Y, Kiper N, Watanabe K, Taniguchi T, Kong J, Tisdale W A, Ashoori R, Gedik N, Fu L, Xu S Y and Jarillo-Herrero P 2020 *Nature* **588** 71

[16] Wang X, Yasuda K, Zhang Y, Liu S, Watanabe K, Taniguchi T, Hone J, Fu L and Jarillo-Herrero P 2022 *Nat. Nanotechnol.* **17** 367
[17] Deb S, Cao W, Raab N, Watanabe K, Taniguchi T, Goldstein M, Kronik L, Urbakh M, Hod O and Ben Shalom M 2022 *Nature* **612** 465
[18] Wei L Q, Zheng Y H, Guan Z, Tong W Y, Fan W C, Xu H W, Sun W H, Cheng Y, Chen B B, Xiang P H, Duan C G, and Zhong N 2026 *Adv. Mater.* **38** e14265
[19] Guan Z, Wei L, Fan W, Sun Y, Cao W, Tian M, Wan N, Tong W, Chen B, Xiang P, Duan C and Zhong N 2025 *Nat. Commun.* **16** 986
[20] Bennett D, Chaudhary G, Slager R J, Bousquet E and Ghosez P 2023 *Nat. Commun.* **14** 1629
[21] Zheng J D, Yao C S, Zhou S C, Zhang Y K, Bao Z Q, Tong W Y, Chu J H and Duan C G 2025 *Adv. Funct. Mater.* **35** 2503011
[22] Qian Z, Gong Z, Li J, Wang H and Liu S 2025 *Chin. Phys. Lett.* **42** 070715
[23] Fei Z, Zhao W, Palomaki T A, Sun B, Miller M K, Zhao Z, Yan J, Xu X and Cobden D H 2018 *Nature* **560** 336
[24] Sharma P, Xiang F X, Shao D F, Zhang D, Tsymbal E Y, Hamilton A R and Seidel J 2020 *Sci. Adv.* **5** eaax5080
[25] Zhu Y, Wang Z G, Ren Y J, Yuan P H, Chen J Z, Ou Y, Meng L L and Zhang Y 2025 *Chin. Phys. B* **34** 017302
[26] Meng P, Wu Y, Bian R, Pan E, Dong B, Zhao X, Chen J, Wu L, Sun Y, Fu Q, Liu Q, Shi D, Zhang Q, Zhang Y W, Liu Z and Liu F 2022 *Nat. Commun.* **13** 7696
[27] Park J, Yeu I W, Han G, Hwang C S and Choi J H 2019 *Sci. Rep.* **9** 14919
[28] Wan Y, Hu T, Mao X, Fu J, Yuan K, Song Y, Gan X, Xu X, Xue M, Cheng X, Huang C, Yang J, Dai L, Zeng H and Kan E 2022 *Phys. Rev. Lett.* **128** 067601
[29] Miao L P, Ding N, Wang N, Shi C, Ye H Y, Li L, Yao Y F, Dong S and Zhang Y 2022 *Nat. Mater.* **21** 1158
[30] Sui F, Jin M, Zhang Y, Qi R, Wu Y N, Huang R, Yue F and Chu J 2023 *Nat. Commun.* **14** 36
[31] Kang K, Li T, Sohn E, Shan J and Mak K F 2019 *Nat. Mater.* **18** 324
[32] Ali M N, Xiong J, Flynn S, Tao J, Gibson Q D, Schoop L M, Liang T, Haldolaarachchige N, Hirschberger M, Ong N P and Cava R J 2014 *Nature* **514** 205
[33] Tang S, Zhang C, Wong D, Pedramrazi Z, Tsai H Z, Jia C, Moritz B, Claassen M, Ryu H, Kahn S, Jiang J, Yan H, Hashimoto M, Lu D, Moore R G, Hwang C C, Hwang C, Hussain Z, Chen Y, Ugeda M M, Liu Z, Xie X, Devereaux T P, Crommie M F, Mo S K and Shen Z X 2017 *Nat. Phys.* **13** 683
[34] Li P, Wen Y, He X, Zhang Q, Xia C, Yu Z M, Yang S A, Zhu Z, Alshareef H N and Zhang X X 2017 *Nat. Commun.* **8** 2150
[35] Song T, Jia Y, Yu G, Tang Y, Wang P, Singha R, Gui X, Uzan-Narovlansky A J, Onyszczak M, Watanabe K, Taniguchi T, Cava R J, Schoop L M, Ong N P and Wu S 2024 *Nat. Phys.* **20** 269
[36] Xiao J, Wang Y, Wang H, Pemmaraju C D, Wang S, Muscher P, Sie E J, Nyby C M, Devereaux T P, Qian X, Zhang X and Lindenberg A M 2020 *Nat. Phys.* **16** 1028
[37] de la Barrera S C, Cao Q, Gao Y, Gao Y, Bheemarasetty V S, Yan J, Mandrus D G, Zhu W, Xiao D and Hunt B M 2021 *Nat. Commun.* **12** 5298
[38] Panasci S E, Schilirò E, Roccaforte F and Giannazzo F 2025 *Adv. Funct. Mater.* **35** 2414532
[39] Velický M, Donnelly G E, Hendren W R, McFarland S, Scullion D, DeBenedetti W J I, Correa G C, Han Y, Wain A J, Hines M A, Muller D A, Novoselov K S, Abruña H D, Bowman R M, Santos E J G and Huang F 2018 *ACS Nano* **12** 10463
[40] Huang Y, Pan Y H, Yang R, Bao L H, Meng L, Luo H L, Cai Y Q, Liu G D, Zhao W J, Zhou Z, Wu L M, Zhu Z L, Huang M, Liu L W, Liu L, Cheng P, Wu K H, Tian S B, Gu C Z, Shi Y G, Guo Y F, Cheng Z G, Hu J P, Zhao L, Yang G H, Sutter E, Sutter P, Wang Y L, Ji W, Zhou X J and Gao H J 2020 *Nat. Commun.* **11** 2453
[41] Chen Y, Peng B, Cong C, Shang J, Wu L, Yang W, Zhou J, Yu P, Zhang H, Wang Y, Zou C, Zhang J, Liu S, Xiong Q, Shao H, Liu Z, Zhang H, Huang W and Yu T 2019 *Adv. Mater.* **31** 1804979
[42] Tiwari A, Chen F, Zhong S, Drueke E, Koo J, Kaczmarek A, Xiao C, Gao J, Luo X, Niu Q, Sun Y, Yan B, Zhao L and Tsen A W 2021 *Nat. Commun.* **12** 2049
[43] Gruverman A, Alexe M and Meier D 2019 *Nat. Commun.* **10** 1661
[44] Liu Y, Collins L, Proksch R, Kim S, Watson B R, Doughty B, Calhoun T R, Ahmadi M, Ievlev A V, Jesse S, Retterer S T, Belianinov A, Xiao K, Huang J, Sumpter B G, Kalinin S V, Hu B and Ovchinnikova O S 2018 *Nat. Mater.* **17** 1013
[45] Guan Z, Jiang Z Z, Tian B B, Zhu Y P, Xiang P H, Zhong N, Duan C G and Chu J H 2017 *AIP Adv.* **7** 095116
[46] Wei L Q, Guan Z, Tong W Y, Fan W C, Mattursun A, Chen B B, Xiang P H, Han G, Duan C G and Zhong N 2024 *Adv. Sci.* **11** 2410354
[47] Ren Z Q, Liu Y D, Bao S Y, Yang N, Zhong N, Tang X D, Xiang P H and Duan C G 2019 *Appl. Phys. Lett.* **115** 242901
[48] Wang J J, Ma R R, Guan Z, Ren Z Q, Zhong N, Xiang P H and Duan C G 2020 *J. Appl. Phys.* **128** 184104
[49] Ye F, Lee J, Hu J, Mao Z, Wei J and Feng P X L 2016 *Small* **12** 5802
[50] Balke N, Maksymovych P, Jesse S, Herklotz A, Tselev A, Eom C B, Kravchenko I I, Yu P and Kalinin S V 2015 *ACS Nano* **9** 6484
[51] Zomer P J, Guimarães M H D, Brant J C, Tombros N and van Wees B J 2014 *Appl. Phys. Lett.* **105** 013101
[52] Li R, Taniguchi T, Watanabe K and Xue J 2020 *Rev. Sci. Instrum.* **91** 073702
[53] Sun X, Chen Y, Li Z, Han Y, Zhou Q, Wang B, Taniguchi T, Watanabe K, Zhao A, Wang J, Liu Y and Xue J 2021 *ACS Nano* **15** 16314
[54] Collins L, Liu Y, Ovchinnikova O S and Proksch R 2019 *ACS Nano* **13** 8055
[55] Litterst M, Butkevich A A and Kemerink M 2025 *Nature* **644** E1
[56] Ganpule C S, Nagarajan V, Ogale S B, Roytburd A L, Williams E D and Ramesh R 2000 *Appl. Phys. Lett.* **77** 3275
[57] Liang L, Pan E, Cao G, Chen J, Wang R, Dong B, Liu Q, Chen X, Luo X, Kong Y, Li W and Liu F 2025 *Nat. Commun.* **16** 4462
[58] McGilly L J, Kerelsky A, Finney N R, Shapovalov K, Shih E M, Ghiotto A, Zeng Y, Moore S L, Wu W, Bai Y, Watanabe K, Taniguchi T, Stengel M, Zhou L, Hone J, Zhu X, Basov D N, Dean C, Dreyer C E and Pasupathy A N 2020 *Nat. Nanotechnol.* **15** 580
[59] Lv M, Sun X, Chen Y, Taniguchi T, Watanabe K, Wu M, Wang J and Xue J 2022 *Adv. Mater.* **34** 2203990
[60] Ke C, Liu F and Liu S 2025 *Phys. Rev. Lett.* **135** 046201
[61] Wang Z and Dong S 2025 *Phys. Rev. B* **111** L201406
[62] Shi Y, Gao Y, Wang H, Zhang B, Zhong Z and He R 2025 *Phys. Rev. B* **112** 035421
[63] Pan E, Li Z, Yang F, Niu K, Bian R, Liu Q, Chen J, Dong B, Wang R, Zhou T, Zhou A, Luo X, Chu J, Lin J, Li W and Liu F 2025 *Nat. Commun.* **16** 3026
[64] He R, Zhang B, Wang H, Li L, Tang P, Bauer G and Zhong Z 2024 *Acta Mater.* **262** 119416
[65] Xu H W, Fan W C, Zheng J D, Yao C S, Zhong N, Tong W Y and Duan C G 2026 *Nano Lett.* **26** 1043
[66] Lv M, Wang J, Tian M, Wan N, Tong W, Duan C and Xue J 2024 *Nat. Commun.* **15** 295
[67] Van Winkle M, Dowlatshahi N, Khaloo N, Iyer M, Craig I M, Dhall R, Taniguchi T, Watanabe K and Bediako D K 2024 *Nat. Nanotechnol.* **19** 751
[68] Ko K, Yuk A, Engelke R, Carr S, Kim J, Park D, Heo H, Kim H M, Kim S G, Kim H, Taniguchi T, Watanabe K, Park H, Kaxiras E, Yang S M, Kim P and Yoo H 2023 *Nat. Mater.* **22** 992
[69] Cao W, Deb S, Stern M V, Raab N, Urbakh M, Hod O, Kronik L and Shalom M B 2024 *Adv. Mater.* **36** 2400750